Interface-Controlled Synthesis of Heterodimeric Silver–Carbon Nanoparticles Derived from Polysaccharides

Yuri Choi,[†] Gyeong Hee Ryu,[‡] Sa Hoon Min,[†] Bo Ram Lee,[‡] Myoung Hoon Song,[‡] Zonghoon Lee,[‡] and Byeong-Su Kim*[,†]

[†]Department of Chemistry and Department of Energy Engineering and [‡]School of Materials Science and Engineering and Low Dimensional Carbon Materials Center, Ulsan National Institute of Science and Technology (UNIST), Ulsan 689-798, Korea

ABSTRACT Hybrid nanoparticles composed of multiple components can offer unique opportunities for understanding the nanoscale mechanism and advanced material applications. Here, we report the synthesis of heterodimeric silver–carbon dot nanoparticles (Ag-CD NPs) where the Ag NP is grown on the surface of CDs derived from polysaccharides, such as chitosan and alginate, through the photoelectron transfer reaction between CD and Ag^+ ions. The nanoscale interface between the Ag NPs and the CDs is highly tunable depending on the precursor of the CDs and the amount of additives, resulting in fine modification of photoluminescence of the CDs as well as the related surface plasmon resonance of the Ag NPs. This result demonstrates the critical role of the interface between the hybrid nanoparticles in governing the electrical and optical properties of respective nanoparticles.

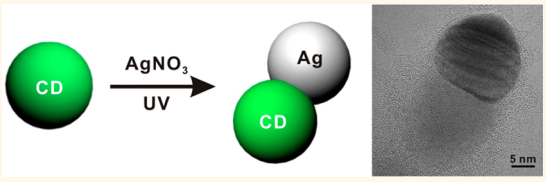

KEYWORDS: carbon dot · heterodimeric nanoparticle · silver nanoparticle · interface

With advances in the synthesis of nanoparticles, hybrid nanoparticles that consist of different components are emerging as an important class of materials.[1,2] These nanoparticles are attracting significant interest because their uniquely integrated multifunctional properties are difficult or even impossible to achieve in single-component nanoparticles. These unique features facilitate the application of hybrid nanoparticles in diverse fields, including catalysis,[3,4] sensors,[5] electronics,[6] diagnosis,[7] and therapy.[8] However, the development of facile strategies for the synthesis of multicomponent hybrid nanoparticles has been challenging. To date, there are a number of reports describing the preparation of complex, multimaterial nanoparticles, including core–shell nanoparticles,[9,10] fused-particle heterostructures,[11−14] segmented nanowires,[15,16] particles coated with other particles,[17,18] yolk–shell nanoparticles,[19−21] and more sophisticated anisotropic structures.[22,23] This recent progress allows for the fabrication of various nanoparticles with unique heterostructures; however, the majority of the hybrid nanoparticles are limited to the combination of noble-metal nanoparticles with magnetic or semiconducting nanoparticles.[24−27]

As a benign alternative to semiconducting quantum dots, carbogenic nanoparticles (also known as carbon dots, CDs) have recently received considerable attention by virtue of their interesting physical, optical, and chemical properties, such as their photoluminescence, photostability, and electron transfer behavior.[28−30] By taking advantages of their interesting photoinduced electron transfer phenomena, we developed a facile synthesis of heterodimeric Ag-CD NPs, where Ag NPs are grown at the interface of CDs that originate from polysaccharides of chitosan and alginate (Figure 1). The interfacial interaction between the Ag NPs and CDs was tuned by changing the CD precursor and the additive during the formation of CDs. The interfaces of the hybrid Ag-CD NPs were characterized with high-resolution transmission electron microscopy (HR-TEM) and electron energy loss spectroscopy (EELS) at atomic scale; the results revealed that

* Address correspondence to bskim19@unist.ac.kr.

Received for review August 1, 2014 and accepted October 16, 2014.

Published online October 16, 2014
10.1021/nn504287q

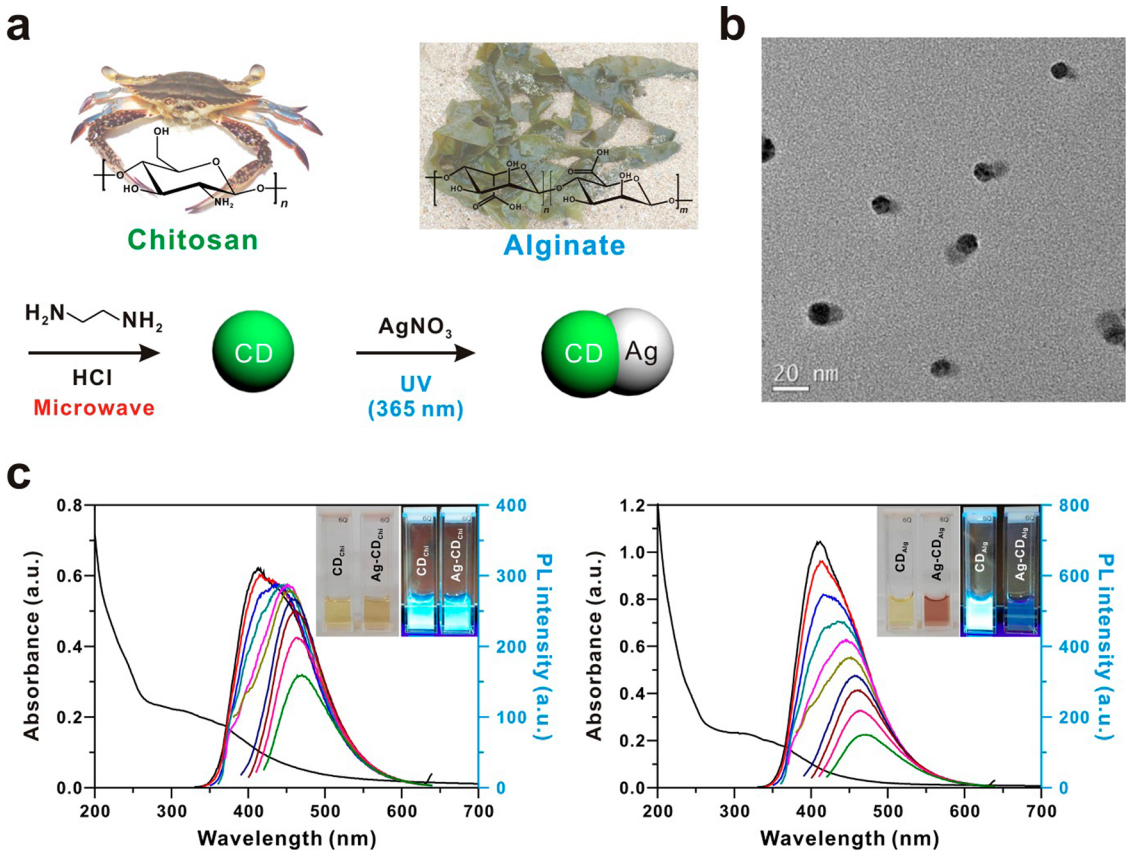

Figure 1. Schematic illustration of the synthesis of heterodimeric Ag-CD NPs derived from polysaccharides. (a) Schematic representation of the synthesis of CD NPs from chitosan and alginate precursors followed by growth of Ag NPs on the CDs. (b) Representative TEM image of the Ag-CD_{Chi} NPs. (c) UV/vis absorption and PL spectra of the CDs in solutions prepared from (left) chitosan (CD_{Chi}) and (right) alginate (CD_{Alg}) with varying excitation wavelengths from 320 to 410 nm with an interval of 10 nm. The inset shows the photographs of the respective CD and Ag-CD NP solutions under ambient light and UV irradiation at 365 nm (concn = 0.10 mg/mL). The samples were prepared with 600 μL of HCl added during the synthesis of the CDs (see Methods section for details).

the metallic Ag NPs were synthesized at the junction of the CDs. The precise tuning of the metal−carbon interface also allows for modification of the photoluminescence (PL) properties of CDs as well as the related surface plasmon resonance (SPR) of the Ag NPs. Although there are some previous reports on the growth of Ag NPs on the CDs including our own approach (Supporting Information Table S1),[31−33] to the best of our knowledge, this work represents the first report of heterodimeric structures from Ag-CD NPs with a controlled nanoscale interface.

RESULTS AND DISCUSSION

Among many synthetic methods available, we employed microwave pyrolysis of chitosan or alginate in the presence of a surface passivating agent (ethylenediamine, $NH_2CH_2CH_2NH_2$) and a solubilizing additive (HCl) to prepare the respective CDs. Each carbon source belongs to a common polysaccharide extracted from biomass, such as crab or brown algae. The prepared CDs are thus denoted as CD_{Chi} and CD_{Alg} depending on the respective carbon precursor. Both CDs exhibit broad absorbance and characteristic PL with emission maxima that are highly dependent on the excitation wavelength similar to other reported CDs.[34,35] The CD_{Chi} generally shows relatively low PL, with a quantum yield (QY) of ~5%, compared to that of CD_{Alg} (QY ~ 10%) using quinine sulfate as a reference. The CDs were subsequently photoexcited by irradiation with UV light in the presence of $AgNO_3$, which led to the formation of Ag NPs on the surface of the CDs upon reduction of Ag^+ ions.[36] The successful formation of Ag NPs was monitored by changes in solution color as well as by the diminished PL under UV light (Figure 1c and Figure S1). Most surprisingly, we found that only a single Ag NP was grown on each CD, as evidenced by the representative TEM image, which resulted exclusively in heterodimeric structures without the formation of other hybrid structures of different morphology (Figure 1). Notably, no Ag NP formation was observed in the absence of the CDs under identical reaction conditions in repeated control experiments.

The mechanism of controlled nucleation and directional growth of Ag NPs can be attributed to the electron transfer between the photoexcited CDs and the Ag^+ ions,

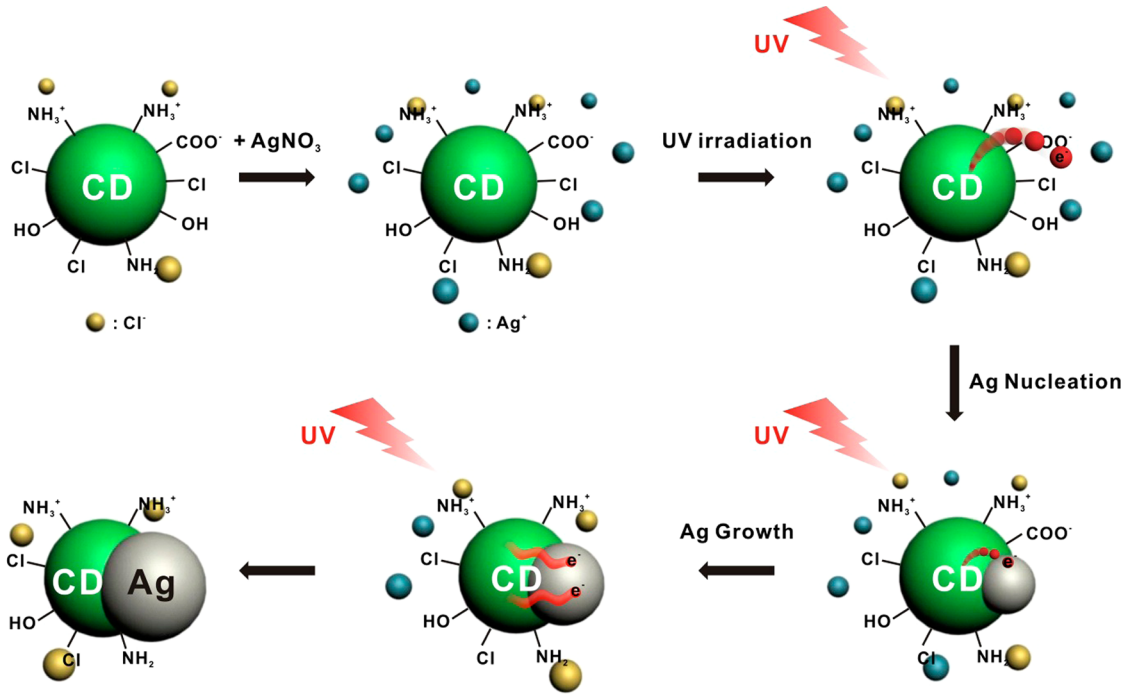

Figure 2. Proposed formation mechanism of heterodimeric Ag-CD NPs.

as similarly suggested in other dumbbell-shaped heterodimers such as Pt—Fe_3O_4 and Au—Fe_3O_4.[37,38] Specifically, Ag^+ ions (and also Cl^- ions) are attracted to the surface of CDs *via* electrostatic interactions with carboxylic acid, amine, and/or other functional groups. After the free electrons from the photoexcited CDs reach the Ag^+ ions at the surface, the interfacial junction allows more electrons to pass through to the conductive Ag nucleation site and to recruit more Ag^+ ions, eventually leading to heterodimeric Ag-CD NPs (Figure 2). Although the literature contains a few previous reports describing the formation of CDs coated with metals such as Ag, Au, and Pt, all of them exhibit core—shell morphology with a CD core and a thin metallic shell.[39,40]

To further support the formation mechanism, we performed FT-IR and high-resolution X-ray photoelectron spectroscopy (XPS). FT-IR spectroscopy revealed chemical information related to the functional groups that change during the course of the reaction (Figure S2). In particular, the fraction of carboxylic acid groups and other oxygen-bearing functional groups were diminished upon the formation of the Ag NPs on the surface of the CDs, irrespective of the type of CD. In accordance with the FT-IR data, XPS results provided further evidence of Ag NP formation and the associated changes in the surface functional groups on the CDs (Figures S3—S5). The survey scan identified the Ag NPs from the Ag 3d peaks at 368.19 and 374.38 eV and the characteristic features of sp^2- and sp^3-carbons that were functionalized with carbonyl and amine moieties on the particle surfaces. Furthermore, the deconvoluted high-resolution C 1s spectra revealed that both sp^2-carbon and hydroxyl groups of the CDs diminished considerably upon the synthesis of the Ag NPs, whereas the carbonyl groups increased concomitantly, suggesting their important role in reducing Ag^+ ions to metallic Ag NPs. Considering this evidence together, we propose that the hydroquinone-like (a combination of sp^2-carbons and hydroxyl groups) surface functional groups of CDs are oxidized to benzoquinone-like structures upon UV irradiation to promote the reduction of Ag^+ ions on the surface of photoexcited CDs (Figure S6). It is worth noting that the high-resolution Cl 2p spectra indicated the presence of C—Cl at 197.9 ($2p_{3/2}$) and 199.6 eV ($2p_{1/2}$), which suggests the Cl atom is incorporated within the carbon framework during the formation of the CD.[41] The presence of C—Cl was further confirmed by FT-IR and elemental mapping data (Figure S2).

The unique structure and interface of heterodimers established between metallic Ag NPs and nonmetallic soft carbon-based CDs were further characterized by high-resolution aberration-corrected TEM operated at a low kilovolts (Figure 3). To enhance the contrast of high-resolution imaging of carbon-based CDs, we used a graphene support transferred onto Quantifoil holey carbon grid (Quantifoil Micromachined, R2/1, SPI supplies). As shown in Figure 3a, the heterodimeric structure of Ag-CD_{Chi} NPs is clearly demonstrated to have crystal lattice fringes of metallic Ag. However, a weak crystalline plane with a spacing of 0.277 nm was observed in the digital diffractogram of the CD, indicating the presence of insoluble AgCl salt on the surface of the CDs, as evidenced by the weak (200) peak. The presence of AgCl corroborates the proposed mechanism by confirming the presence of Cl^- ions on

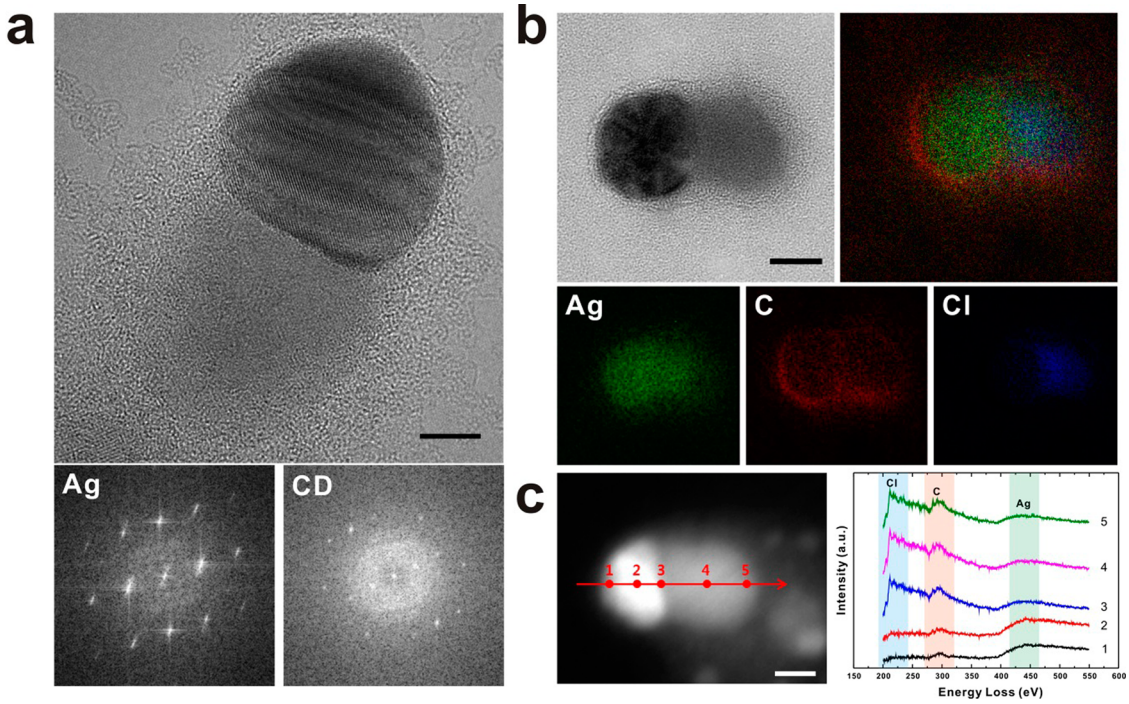

Figure 3. Representative high-resolution TEM images of Ag-CD_{Chi} NPs. (a) Aberration-corrected TEM image of Ag-CD_{Chi} NPs (scale bar: 5 nm) and the corresponding digital diffractograms of the Ag NPs and the CD. (b) Energy-filtered TEM image of Ag-CD_{Chi} NPs (scale bar: 10 nm) with composed elemental images of Ag, C, and Cl. (c) STEM-HAADF image of Ag-CD_{Chi} NPs (scale bar: 10 nm) and the corresponding monochromated STEM-EEL spectra of points along the line on a heterodimeric Ag-CD_{Chi} NP. Notably, the remaining carbon residue could be due to the preparation of the sample on a graphene substrate, or the TEM measurement might induce carbon peaks around the surface of the heterodimer.

the surface of the CDs through the electrostatic interaction with amine groups on the surface functional groups of the CDs and the associated Ag^+ ions. A control experiment using acetic acid as an additive instead of HCl also produced the heterodimeric Ag-CD_{Chi} NPs, suggesting the role of H^+ in forming the nanostructures (Figures S7 and S8). Furthermore, the crystalline phase of the Ag-CD NPs was verified by the XRD spectrum (Figure S9). The associated elemental information on heterodimers was elucidated by energy-filtered TEM (EFTEM) and monochromated electron energy loss spectroscopy (mono-EELS) (Figure 3b,c). The EFTEM image shows the distribution of each element—Ag, C, and Cl—on the heterodimer. As shown in Figure 3b, the Ag is localized on the Ag NP, whereas the C and Cl are mostly distributed on the CD. The monochromated STEM-EEL spectra of points along the line on heterodimeric Ag-CD_{Chi} NPs also reveal elemental concentration information related to the respective NPs on the basis of the C K-edge (285 eV), the Cl $L_{2,3}$-edge (200 eV), and the Ag $M_{4,5}$-edge (367 eV). Taken together, the high-resolution TEM, along with a number of other analytical analyses, supports the successful formation of heterodimeric Ag-CD NPs.

We found that the concentration of HCl added during the formation of the CDs is a critical parameter in controlling the size and the interface of Ag-CDs. The addition of HCl assists in enhancing the solubility of chitosan and alginate in aqueous solutions for the synthesis of CDs, and Cl^- ions in the resulting solution also affect the growth kinetics of Ag NPs during heterodimer formation. A series of TEM images shown in Figure 4 indicate that an increase in the concentration of HCl increases the size of the CDs. For example, the size of CD_{Chi} increased from 7.90 ± 0.73 to 13.1 ± 0.56 nm when the amount of 1 M HCl was changed from 200 to 1000 μL; similarly, the size of CD_{Alg} increased from 7.14 ± 0.87 to 13.1 ± 1.29 nm under identical conditions (Figure 4c). In addition, the size of the Ag NPs increased with increased concentration of HCl in both CDs. Interestingly, we found that the aspect ratio of CD_{Alg} in Ag-CD_{Alg} gradually increased with increasing HCl concentration, whereas that of CD_{Chi} in Ag-CD_{Chi} NPs remained almost constant (Figure 4d).

Most notably, the concentration of HCl can enable the fine-tuning of the interface between two components of the heterodimers (Figure 4e). Through the collection of a series of TEM images, we could clearly monitor the gradual changes of the overlapped area between the Ag and CD NPs (Figures S10 and S11). For instance, the eclipsing of the Ag and CD_{Chi} NPs at the interface was significantly reduced with increasing concentration of the HCl additive. In stark contrast, the trend was reversed in the case of Ag-CD_{Alg} NPs, such that the eclipsing between Ag and CD_{Alg} NPs increased with increasing concentration of HCl. We propose that the protonation of the chitosan precursor bearing amine groups affords greater solubilization of the chitosan

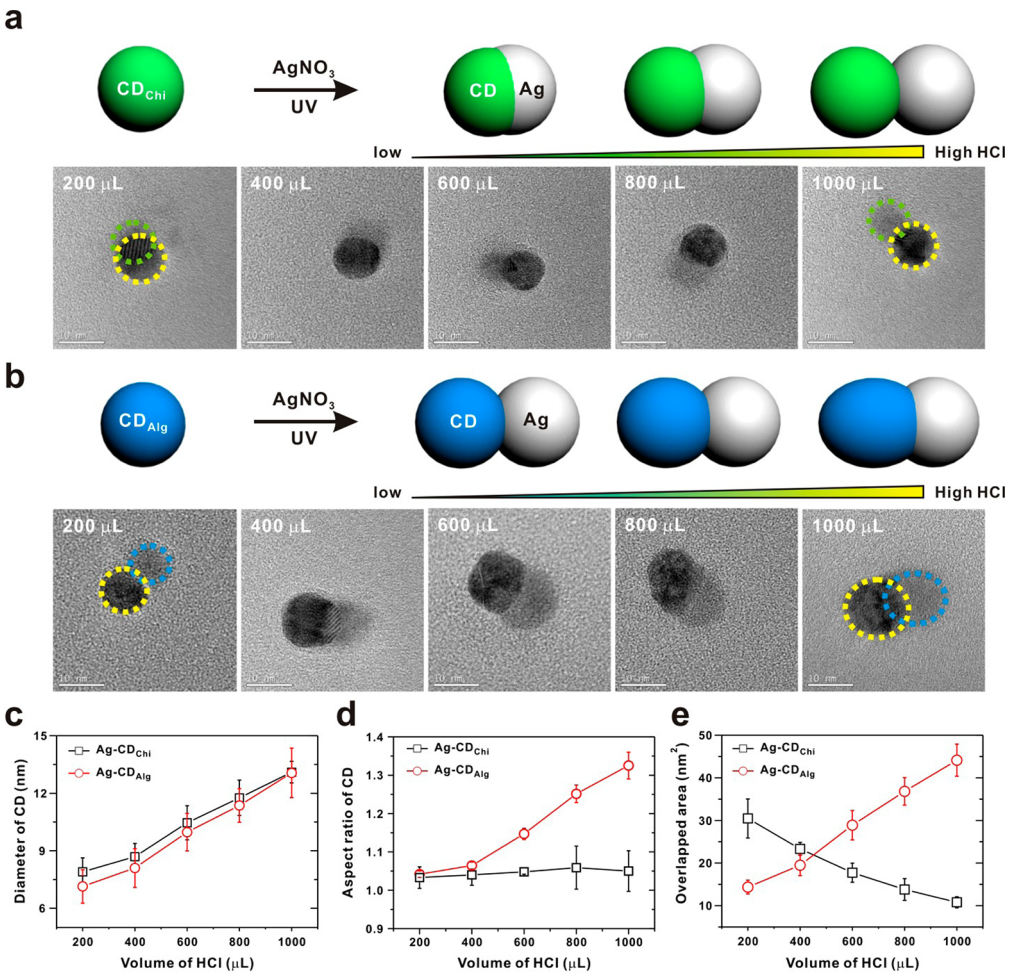

Figure 4. Effect of the HCl additive on tuning the nanoscale interface of the Ag-CD NPs. (a,b) Representative TEM images of (a) Ag-CD$_{Chi}$ NPs and (b) Ag-CD$_{Alg}$ NPs prepared with various amounts of 1 M HCl additive, as indicated in the image. Dotted lines were added to aid the identification of each NP. (c–e) Analysis of characteristics of the Ag-CD NPs. (c) Diameter of CDs in Ag-CD NPs, (d) aspect ratio of CDs in Ag-CD NPs, and (e) overlapped interfacial area of Ag and CD in Ag-CD$_{Chi}$ and Ag-CD$_{Alg}$ NPs. All analyses are reported as an average value of more than 50 individual measurements of TEM images, and error bars indicate the standard deviations.

precursor upon addition of HCl to the mixture. However, the opposite behavior was observed when the carboxylic acid groups on the alginate were treated with HCl. This opposite solubility trend of the two polysaccharides might lead to differences in the synthesis of CDs during the microwave carbonization. The fine structural tuning of the Ag NP and CD interface enables surface modification of the CDs and also changes the related optical properties of the Ag and CD NPs, such as the PL of CDs and the SPR of Ag NPs.

We performed various characterizations of all the Ag-CDs prepared using various amounts of HCl, including steady-state photoluminescence spectroscopy, time-correlated single-photon counting (TCSPC), and QY measurements, to elucidate the effect of structural tuning of the Ag and CD NPs on their photophysical properties (Figure 5). The PL decay profiles of Ag-CD$_{Chi}$ and Ag-CD$_{Alg}$ NPs show a shorter decay lifetime compared to their counterpart CDs without Ag NPs, which can be deduced to fit biexponential decay parameters. From the fitting of the decay curves of representative 600 μL HCl samples, the average PL decay time of τ_{avg} (the exciton lifetime) was calculated to be 4.14 ns for Ag-CD$_{Chi}$ and 2.58 ns for Ag-CD$_{Alg}$, which are shorter than those of the respective CDs free of Ag NPs: 4.39 ns for CD$_{Chi}$ and 4.62 ns for CD$_{Alg}$ (Table S2). In general, the PL of CDs is attributed to radiative combinations of electrons and holes confined at the defective surfaces of CDs.[28,42] The exciton created on the surface of the CDs can be effectively quenched by the presence of neighboring metallic Ag NPs. Consequently, the lifetime of the exciton is decreased accordingly and is also highly dependent on the interparticle spacing between the CD and Ag NPs. As indicated by the opposite trend of interfacial overlapping between Ag-CD$_{Chi}$ and Ag-CD$_{Alg}$ NPs, the τ_{avg} of the Ag-CD$_{Chi}$ NPs generally increases with decreasing overlap between the Ag and CD$_{Chi}$, whereas that tendency is reversed in the case of Ag-CD$_{Alg}$. Figure 5c,d shows the QYs of the CD and Ag-CD NP suspensions, which are in excellent agreement

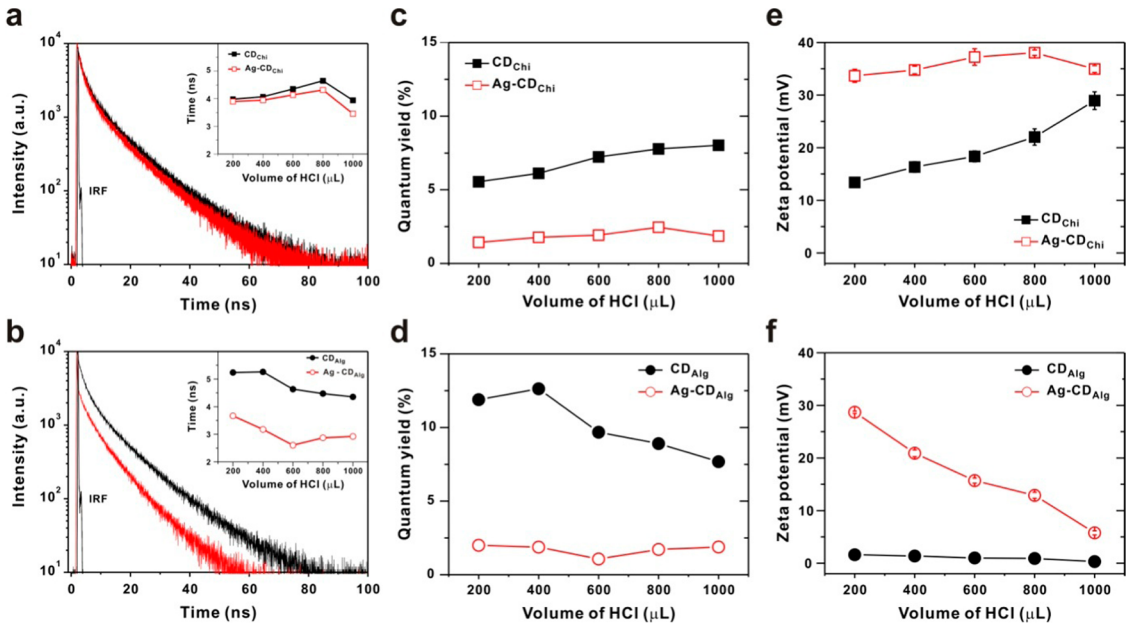

Figure 5. Photophysical properties and stability of Ag-CD NPs. (a,b) Photoluminescence decay profiles of (a) Ag-CD_{Chi} NPs and (b) Ag-CD_{Alg} NPs prepared with 600 μL of HCl. The inset shows the plot of the average decay time (τ_{avg}) of CDs (black) and Ag-CDs (red) as a function of the volume of HCl. (c,d) Quantum yields of CD and Ag-CD NP solutions, respectively, measured with quinine sulfate as a reference material. (e,f) Zeta-potentials of CD and Ag-CD NP suspensions, respectively.

with the PL lifetime decay values. Sun and co-workers have reported that the deposition of metallic Au NPs around CDs effectively quenches or almost diminishes the PL in the CDs to a concentration far below the threshold of observation for plasmon absorption.[40] However, these heterodimeric Ag-CD NPs are unique in that the presence of the Ag NPs does not completely quench the PL of native CDs because of the controlled interface of the heterodimeric nanostructure. Independent of the PL measurements, we measured the zeta-potential of the NPs and found that the CDs and Ag-CD NPs all exhibited good colloidal stability that lasted for several months without any noticeable aggregation (Figure 5e,f). Due to amine groups of chitosan and carboxylic groups of alginate precursors, the zeta-potential of CD_{Chi} has relatively higher values (more positively charged) than CD_{Alg}. Because the formation of heterodimeric Ag NPs on the surface of CDs requires the consumption of surface carboxylic acid and hydroxyl groups, the more overlapped area between Ag and CDs can lead to considerable changes in the zeta-potential of Ag-CD NPs. For example, we found that more oxygenated CD_{Alg} (34.2%, according to XPS data) compared to CD_{Chi} (25.3%) provided more active sites, thus leading to the rapid formation of Ag NPs in CD_{Alg}, which significantly increased the zeta-potential of Ag-CD_{Alg} NPs. These results clearly confirm that the nanoscale interface between Ag and CDs can be controlled precisely through the choice of the CD precursor and the additive.

Because SPR of metallic NPs is well-known to be highly sensitive to the dielectric environment, the formation of Ag NPs on dielectric CDs with tunable interparticle spacing can significantly influence the local field generated by the Ag NPs. Thus, we simulated the electric field distribution using the three-dimensional finite-difference time-domain (FDTD) method to explore the electric field enhancement created at the junction of the heterodimeric Ag-CD NPs (Figure 6).[43] Figure 6 presents the simulated electric field intensity distribution and predicts the extinction spectra of representative Ag-CD_{Chi} NPs with varying degrees of interparticle spacing (200, 600, and 1000 μL of 1 M HCl). The overlapped area between Ag and CD_{Chi} decreases with increasing concentration of HCl in the case of Ag-CD_{Chi}; hence, we performed the simulation according to the data set collected from TEM images. We observed that less eclipsing of the Ag with the CD surface makes the electronic coupling of the Ag and CD NPs stronger, which leads to a significant electric field enhancement at the junction between the Ag and CD NPs (Figure 6b). In addition, the simulated extinction spectra are red-shifted with less overlap between the Ag and CD NPs, which is consistent with the UV/vis spectroscopy observations (Figure 6c). This simulation demonstrates that fine-tuning the interface between a dielectric material, a CD, and a metallic Ag NP can provide a unique means to control the SPR of Ag NPs.

CONCLUSION

In summary, we synthesized heterodimeric Ag-CD NPs using the photoelectron transfer reaction of polysaccharide-derived CDs to Ag^+ ions. The interface between the Ag NPs and the CDs was precisely tunable through the choice of CD precursor and the amount of additive used during the formation of the CDs.

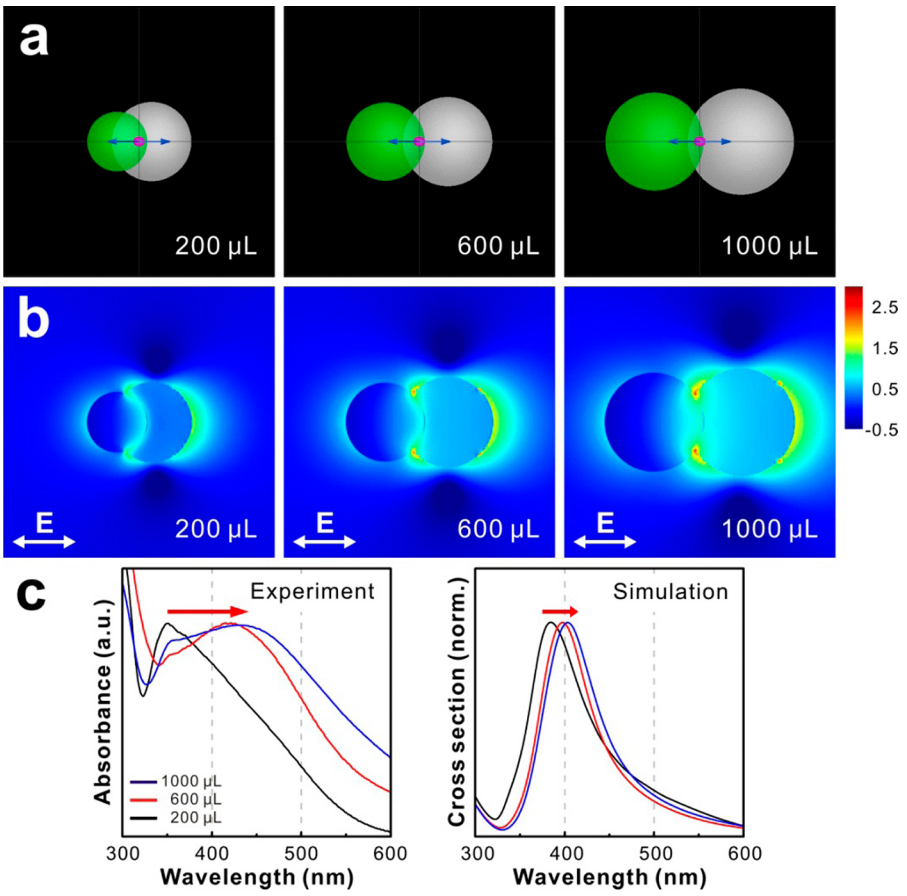

Figure 6. Simulation of the electric field distribution and extinction cross section for Ag-CD_{Chi}. (a) Three-dimensional structures of Ag-CD_{Chi} NPs based on TEM images are modeled for FDTD simulation. The blue arrow and purple point indicate the direction of polarization and propagation of the source, respectively. (b) Simulated electric field intensity of Ag-CD_{Chi} NPs at 453 nm in log scale log($|E|^2$) collected with various amounts of HCl. The magnitude of the enhanced intensity is represented by the color scale. All calculations were performed for samples in water medium. (c) Comparison of the UV/vis spectra and the simulation data collected for Ag-CD_{Chi} NPs. The surface plasmon resonance bands are red-shifted from 350 to 432 nm in experiments and from 385 to 404 nm in FDTD calculations with increasing amounts of HCl.

The hybrid Ag-CD NPs were characterized with various techniques, including UV/vis, PL, FT-IR, XPS, HR-TEM, EELS, TCSPC, and zeta-potential measurements as well as FDTD simulations, which all indicated the formation Ag NPs at the junction of the CDs. Moreover, the precise tuning of the metal and carbon interface also enabled modification of the PL of the CDs as well as the related SPR of the Ag NPs. We anticipate that the electron transfer and surface plasmonic effect of these heterodimers will find their applications in the energy conversion systems or catalysts such as solar cells, electrocatalysts, and photocatalysts.

METHODS

Materials. Chitosan (M_w = 210 000), alginic acid sodium salt, ethylenediamine (99%) (EDA), and hydrobromic acid (48%) were purchased from Sigma-Aldrich. Hydrochloric acid (35%) was purchased from Daejung Chemical.

Synthesis of Carbon Dot Nanoparticles (CDs). CDs were initially synthesized by dehydrating carbohydrates using a commercial household microwave (700 W). To make CD_{Chi}, 9 mg of chitosan (0.052 mmol) was diluted with 10 mL of water, and then different volumes (200 to 1000 μL) of 1.0 M HCl were added to dissolve the chitosan in the water. The solution was subsequently mixed with 694 μL of EDA (10.4 mmol) under vigorous stirring for 2 min. The solution was placed into a microwave oven and heated for 2 min. When the solution cooled to room temperature, a red-brown solid was obtained, which was dissolved in 2 mL of water and filtered with a syringe filter (0.45 μm) to remove salt and unreacted chitosan. CD_{Alg} was obtained by an identical protocol with alginate substituted for the chitosan. CD_{Chi} was also prepared with the additives of 1 M HBr or CH_3CO_2H instead of 1 M HCl using the same procedure.

Synthesis of Ag-CD NPs. Solutions of 3.0 mg/mL of CD_{Chi} and 1.0 mg/mL of $AgNO_3$ were exposed to UV light with a wavelength of 365 nm for 3 min using a UV lamp (B-100AP high-intensity UV lamp, 100 W). Ag-CD_{Alg} was obtained by an identical protocol using CD_{Alg}. After the solution was irradiated with UV light for 3 min, its color changed from light-yellow to orange (Ag-CD_{Chi}) or red (Ag-CD_{Alg}).

Time-Correlated Single-Photon Counting Characterization. The exciton lifetime was determined by the time-correlated single-photon counting technique. A computer-controlled diode laser with a 375 nm wavelength, a 54 ps pulse width, and a 40 MHz repetition rate was used as an excitation source. The PL emission was spectrally resolved using collection optics and a monochromator (PicoQuant). The TCSPC module (PicoHarp

300E, PicoQuant) with a MCP-PMT (R3809U-5x series, Hamamatsu) was used for ultrafast detection. The total instrument response function (IRF) for PL decay was less than 30 ps, and the temporal time resolution was less than 10 ps. The deconvolution of actual fluorescence decay and IRF was performed using fitting software (FlouFit, PicoQuant) to deduce the time constant associated with each exponential decay.

Characterization. The functional groups of the CDs and the Ag-CD NPs were analyzed by XPS (K-alpha, Thermo Fisher) and FT-IR (Varian, Cray 660). UV/vis absorption spectra and photoluminescence emission were measured on a Varian Cary 5000 spectrophotometer. The zeta-potential of colloidal suspensions was measured using a zeta-potential analyzer (Malvern, Zetasizer Nano-ZS). The morphology and size of Ag-CD NPs were measured using transmission electron microscopy (TEM, JEOL JEM-2100, accelerating voltage of 200 kV). The higher-resolution imaging, EFTEM elemental analysis, and high-energy resolution EEL spectroscopy with a monochromator and Quantum GIF 965 of Ag-CD NPs were performed in aberration-corrected TEM (FEI Titan3 G2 60−300 at 80 kV). A low kilovolt operation of TEM and STEM (scanning TEM) significantly reduced the electron beam damage onto the specimens. X-ray diffraction (XRD) measurements were performed on a high-resolution X-ray diffractometer (Bruker Co.).

Finite-Difference Time-Domain Calculations. The E-field enhancement and extinction cross section for Ag-CD NPs were calculated by FDTD method (FDTD Solutions 8.6, Lumerical). The numerical simulations were performed in three-dimensional box which has a cell size of 0.1 nm with perfectly matched layers for all boundaries. For the Ag-CD NP model, their diameter and interparticle spacing were adjusted according to the TEM observation. The dielectric functions of Ag and CD in the UV/vis region were described by a multicoefficient fitted model of the experimental data by Palik.[44] The Ag-CDs were illuminated by a total-field scattered-field plane wave source to obtain the extinction cross section as a function of wavelength by calculating the absorption and scattering cross sections.

Conflict of Interest: The authors declare no competing financial interest.

Acknowledgment. This work was supported by the National Research Foundation of Korea (NRF) grant funded by the Korean government (2010-0028684, 2012R1A1A2040782, and 2012M3A7B4049807).

Supporting Information Available: Additional figures and tables. This material is available free of charge *via* the Internet at http://pubs.acs.org.

REFERENCES AND NOTES

1. Costi, R.; Saunders, A. E.; Banin, U. Colloidal Hybrid Nanostructures: A New Type of Functional Materials. *Angew. Chem., Int. Ed.* **2010**, *49*, 4878–4897.
2. Cortie, M. B.; McDonagh, A. M. Synthesis and Optical Properties of Hybrid and Alloy Plasmonic Nanoparticles. *Chem. Rev.* **2011**, *111*, 3713–3735.
3. Sasaki, K.; Naohara, H.; Choi, Y. M.; Cai, Y.; Chen, W. F.; Liu, P.; Adzic, R. R. Highly Stable Pt Monolayer on PdAu Nanoparticle Electrocatalysts for the Oxygen Reduction Reaction. *Nat. Commun.* **2012**, *3*, 1115.
4. Wang, D. L.; Xin, H. L. L.; Hovden, R.; Wang, H. S.; Yu, Y. C.; Muller, D. A.; DiSalvo, F. J.; Abruna, H. D. Structurally Ordered Intermetallic Platinum−Cobalt Core−Shell Nanoparticles with Enhanced Activity and Stability as Oxygen Reduction Electrocatalysts. *Nat. Mater.* **2013**, *12*, 81–87.
5. Ibanez, F. J.; Zamborini, F. P. Reactivity of Hydrogen with Solid-State Films of Alkylamine- and Tetraoctylammonium Bromide-Stabilized Pd, PdAg, and PdAu Nanoparticles for Sensing and Catalysis Applications. *J. Am. Chem. Soc.* **2008**, *130*, 622–633.
6. Heo, M.; Cho, H.; Jung, J. W.; Jeong, J. R.; Park, S.; Kim, J. Y. High-Performance Organic Optoelectronic Fevices Enhanced by Surface Plasmon Resonance. *Adv. Mater.* **2011**, *23*, 5689–5693.
7. Gao, J. H.; Liang, G. L.; Cheung, J. S.; Pan, Y.; Kuang, Y.; Zhao, F.; Zhang, B.; Zhang, X. X.; Wu, E. X.; Xu, B. Multifunctional Yolk−Shell Nanoparticles: A Potential MRI Contrast and Anticancer Agent. *J. Am. Chem. Soc.* **2008**, *130*, 11828–11833.
8. Cho, N. H.; Cheong, T. C.; Min, J. H.; Wu, J. H.; Lee, S. J.; Kim, D.; Yang, J. S.; Kim, S.; Kim, Y. K.; Seong, S. Y. A Multifunctional Core−Shell Nanoparticle for Dendritic Cell-Based Cancer Immunotherapy. *Nat. Nanotechnol.* **2011**, *6*, 675–682.
9. Dabbousi, B. O.; Rodriguez-Viejo, J.; Mikulec, F. V.; Heine, J. R.; Mattoussi, H.; Ober, R.; Jensen, K. F.; Bawendi, M. G. (CdSe)ZnS Core−Shell Quantum Dots: Synthesis and Characterization of a Size Series of Highly Luminescent Nanocrystallites. *J. Phys. Chem. B* **1997**, *101*, 9463–9475.
10. Shevchenko, E. V.; Bodnarchuk, M. I.; Kovalenko, M. V.; Talapin, D. V.; Smith, R. K.; Aloni, S.; Heiss, W.; Alivisatos, A. P. Gold/Iron Oxide Core/Hollow-Shell Nanoparticles. *Adv. Mater.* **2008**, *20*, 4323–4329.
11. Gu, H. W.; Zheng, R. K.; Zhang, X. X.; Xu, B. Facile One-Pot Synthesis of Bifunctional Heterodimers of Nanoparticles: A Conjugate of Quantum Dot and Magnetic Nanoparticles. *J. Am. Chem. Soc.* **2004**, *126*, 5664–5665.
12. Chen, J. Y.; Wiley, B.; McLellan, J.; Xiong, Y. J.; Li, Z. Y.; Xia, Y. N. Optical Properties of Pd−Ag and Pt−Ag Nanoboxes Synthesized *via* Galvanic Replacement Reactions. *Nano Lett.* **2005**, *5*, 2058–2062.
13. Saunders, A. E.; Popov, I.; Banin, U. Synthesis and Characterization of Organic-Soluble Ag/AgBr Dimer Nanocrystals. *Z. Anorg. Allg. Chem.* **2007**, *633*, 2414–2419.
14. Lee, H. J.; Habas, S. E.; Somorjai, G. A.; Yang, P. D. Localized Pd Overgrowth on Cubic Pt Nanocrystals for Enhanced Electrocatalytic Oxidation of Formic Acid. *J. Am. Chem. Soc.* **2008**, *130*, 5406–5407.
15. Gudiksen, M. S.; Lieber, C. M. Diameter-Selective Synthesis of Semiconductor Nanowires. *J. Am. Chem. Soc.* **2000**, *122*, 8801–8802.
16. Qin, L. D.; Park, S.; Huang, L.; Mirkin, C. A. On-Wire Lithography. *Science* **2005**, *309*, 113–115.
17. Zhu, C.; Zeng, J.; Tao, J.; Johnson, M. C.; Schmidt-Krey, I.; Blubaugh, L.; Zhu, Y. M.; Gu, Z. Z.; Xia, Y. N. Kinetically Controlled Overgrowth of Ag or Au on Pd Nanocrystal Seeds: From Hybrid Dimers to Nonconcentric and Concentric Bimetallic Nanocrystals. *J. Am. Chem. Soc.* **2012**, *134*, 15822–15831.
18. Yang, J.; Ying, J. Y. A General Phase-Transfer Protocol for Metal Ions and Its Application in Nanocrystal Synthesis. *Nat. Mater.* **2009**, *8*, 683–689.
19. Gao, J. H.; Liang, G. L.; Zhang, B.; Kuang, Y.; Zhang, X. X.; Xu, B. FePt@CoS_2 Yolk−Shell Nanocrystals as a Potent Agent To Kill HeLa Cells. *J. Am. Chem. Soc.* **2007**, *129*, 1428–1433.
20. Wu, X. J.; Xu, D. S. Formation of Yolk/SiO_2 Shell Structures Using Surfactant Mixtures as Template. *J. Am. Chem. Soc.* **2009**, *131*, 2774–2775.
21. Seh, Z. W.; Li, W. Y.; Cha, J. J.; Zheng, G. Y.; Yang, Y.; McDowell, M. T.; Hsu, P. C.; Cui, Y. Sulphur-TiO_2 Yolk−Shell Nanoarchitecture with Internal Void Space for Long-Cycle Lithium−Sulphur Batteries. *Nat. Commun.* **2013**, *4*, 1331.
22. Mokari, T.; Sztrum, C. G.; Salant, A.; Rabani, E.; Banin, U. Formation of Asymmetric One-Sided Metal-Tipped Semiconductor Nanocrystal Dots and Rods. *Nat. Mater.* **2005**, *4*, 855–863.
23. Buck, M. R.; Bondi, J. F.; Schaak, R. E. A Total-Synthesis Framework for the Construction of High-Order Colloidal Hybrid Nanoparticles. *Nat. Chem.* **2012**, *4*, 37–44.
24. Gu, H. W.; Yang, Z. M.; Gao, J. H.; Chang, C. K.; Xu, B. Heterodimers of Nanoparticles: Formation at a Liquid−Liquid Interface and Particle-Specific Surface Modification by Functional Molecules. *J. Am. Chem. Soc.* **2005**, *127*, 34–35.
25. Wang, C.; Daimon, H.; Sun, S. H. Dumbbell-like Pt-Fe_3O_4 Nanoparticles and Their Enhanced Catalysis for Oxygen Reduction Reaction. *Nano Lett.* **2009**, *9*, 1493–1496.
26. Gao, J. H.; Gu, H. W.; Xu, B. Multifunctional Magnetic Nanoparticles: Design, Synthesis, and Biomedical Applications. *Acc. Chem. Res.* **2009**, *42*, 1097–1107.

27. Wang, C.; Xu, C. J.; Zeng, H.; Sun, S. H. Recent Progress in Syntheses and Applications of Dumbbell-like Nanoparticles. *Adv. Mater.* **2009**, *21*, 3045–3052.
28. Sun, Y. P.; Zhou, B.; Lin, Y.; Wang, W.; Fernando, K. A. S.; Pathak, P.; Meziani, M. J.; Harruff, B. A.; Wang, X.; Wang, H. F.; *et al.* Quantum-Sized Carbon Dots for Bright and Colorful Photoluminescence. *J. Am. Chem. Soc.* **2006**, *128*, 7756–7757.
29. Baker, S. N.; Baker, G. A. Luminescent Carbon Nanodots: Emergent Nanolights. *Angew. Chem., Int. Ed.* **2010**, *49*, 6726–6744.
30. Li, H. T.; Kang, Z. H.; Liu, Y.; Lee, S. T. Carbon Nanodots: Synthesis, Properties and Applications. *J. Mater. Chem.* **2012**, *22*, 24230–24253.
31. Shen, L. M.; Chen, M. L.; Hu, L. L.; Chen, X. W.; Wang, J. H. Growth and Stabilization of Silver Nanoparticles on Carbon Dots and Sensing Application. *Langmuir* **2013**, *29*, 16135–16140.
32. Liu, M. M.; Chen, W. Green Synthesis of Silver Nanoclusters Supported on Carbon Nanodots: Enhanced Photoluminescence and High Catalytic Activity for Oxygen Reduction Reaction. *Nanoscale* **2013**, *5*, 12558–12564.
33. Choi, H.; Ko, S. J.; Choi, Y.; Joo, P.; Kim, T.; Lee, B. R.; Jung, J. W.; Choi, H. J.; Cha, M.; Jeong, J. R.; *et al.* Versatile Surface Plasmon Resonance of Carbon-Dot-Supported Silver Nanoparticles in Polymer Optoelectronic Devices. *Nat. Photonics* **2013**, *7*, 732–738.
34. Qu, S. N.; Wang, X. Y.; Lu, Q. P.; Liu, X. Y.; Wang, L. J. A Biocompatible Fluorescent Ink Based on Water-Soluble Luminescent Carbon Nanodots. *Angew. Chem., Int. Ed.* **2012**, *51*, 12215–12218.
35. Zhu, S. J.; Meng, Q. N.; Wang, L.; Zhang, J. H.; Song, Y. B.; Jin, H.; Zhang, K.; Sun, H. C.; Wang, H. Y.; Yang, B. Highly Photoluminescent Carbon Dots for Multicolor Patterning, Sensors, and Bioimaging. *Angew. Chem., Int. Ed.* **2013**, *52*, 3953–3957.
36. Wang, X.; Cao, L.; Lu, F. S.; Meziani, M. J.; Li, H.; Qi, G.; Zhou, B.; Harruff, B. A.; Kermarrec, F.; Sun, Y. P. Photoinduced Electron Transfers with Carbon Dots. *Chem. Commun.* **2009**, *45*, 3774–3776.
37. Wang, C.; Wei, Y. J.; Jiang, H. Y.; Sun, S. H. Tug-of-War in Nanoparticles: Competitive Growth of Au on Au-Fe_3O_4 Nanoparticles. *Nano Lett.* **2009**, *9*, 4544–4547.
38. Wang, C.; Yin, H. F.; Dai, S.; Sun, S. H. A General Approach to Noble Metal-Metal Oxide Dumbbell Nanoparticles and Their Catalytic Application for CO Oxidation. *Chem. Mater.* **2010**, *22*, 3277–3282.
39. Cao, L.; Sahu, S.; Anilkumar, P.; Bunker, C. E.; Xu, J. A.; Fernando, K. A. S.; Wang, P.; Guliants, E. A.; Tackett, K. N.; Sun, Y. P. Carbon Nanoparticles as Visible-Light Photocatalysts for Efficient CO_2 Conversion and Beyond. *J. Am. Chem. Soc.* **2011**, *133*, 4754–4757.
40. Xu, J.; Sahu, S.; Cao, L.; Bunker, C. E.; Peng, G.; Liu, Y. M.; Fernando, K. A. S.; Wang, P.; Guliants, E. A.; Meziani, M. J.; *et al.* Efficient Fluorescence Quenching in Carbon Dots by Surface-Doped Metals-Disruption of Excited State Redox Processes and Mechanistic Implications. *Langmuir* **2012**, *28*, 16141–16147.
41. Papirer, E.; Lacroix, R.; Donnet, J. B.; Nanse, G.; Fioux, P. XPS Study of the Halogenation of Carbon Black-Part 2. Chlorination. *Carbon* **1995**, *33*, 63–72.
42. Cao, L.; Wang, X.; Meziani, M. J.; Lu, F. S.; Wang, H. F.; Luo, P. J. G.; Lin, Y.; Harruff, B. A.; Veca, L. M.; Murray, D.; *et al.* Carbon Dots for Multiphoton Bioimaging. *J. Am. Chem. Soc.* **2007**, *129*, 11318–11319.
43. Wen, F. F.; Ye, J.; Liu, N.; Van Dorpe, P.; Nordlander, P.; Halas, N. J. Plasmon Transmutation: Inducing New Modes in Nanoclusters by Adding Dielectric Nanoparticles. *Nano Lett.* **2012**, *12*, 5020–5026.
44. Palik, E. D. Handbook of the Optical Constants of Solids; Academic Press: New York, 1985.